Figure S1

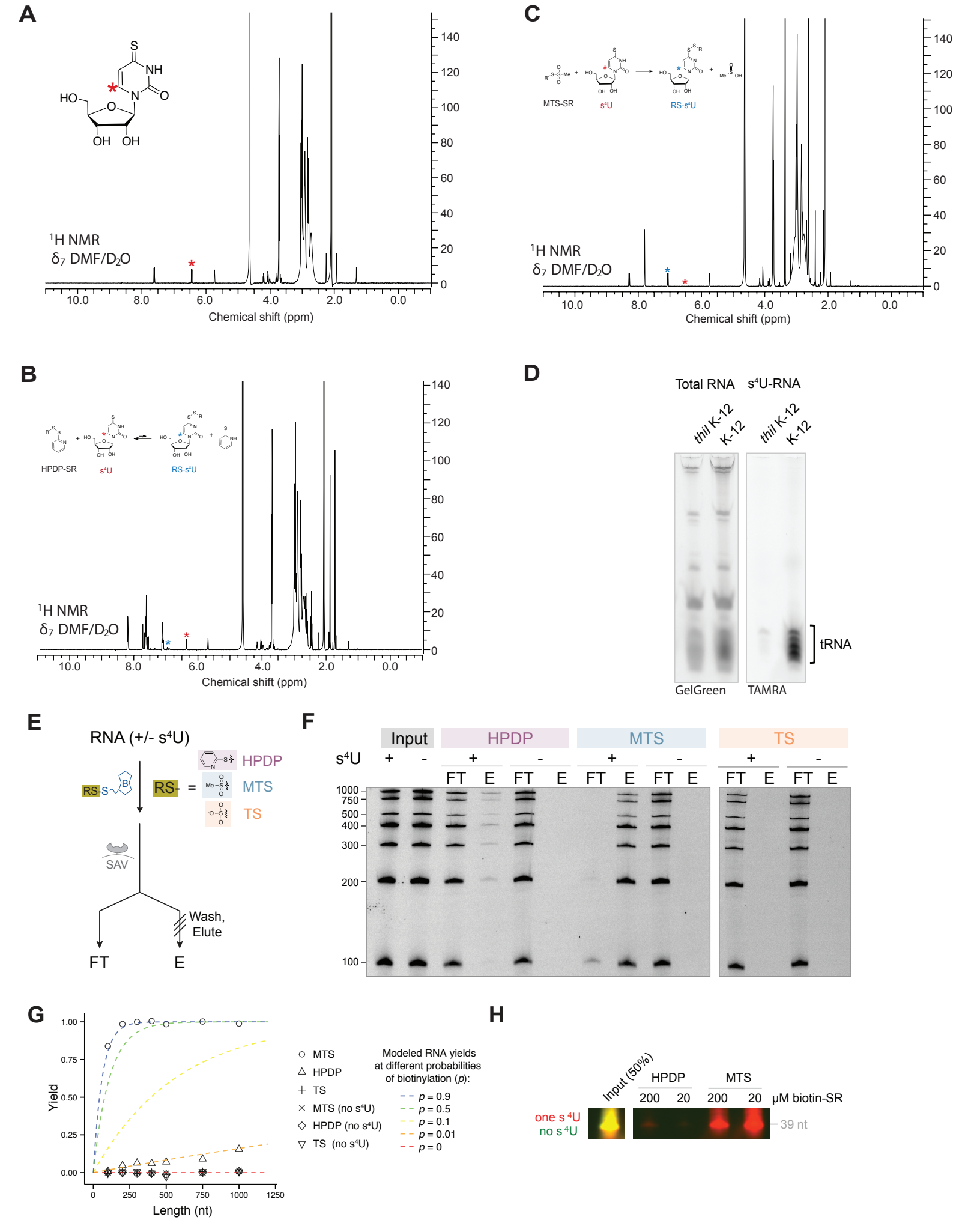
A
B
C
D
E
F
G
H
^{1}H NMR
δ_7 DMF/D_2O
Chemical shift (ppm)
MTS-SR
HPDP-SR
s^{4}U
RS-s^{4}U
Total RNA
s^{4}U-RNA
thiI K-12
K-12
GelGreen
TAMRA
tRNA
RNA (+/- s^{4}U)
HPDP
MTS
TS
SAV
Wash,
Elute
FT
E
Input
s^{4}U
Yield
Length (nt)
Modeled RNA yields
at different probabilities
of biotinylation (p):
p = 0.9
p = 0.5
p = 0.1
p = 0.01
p = 0
MTS
HPDP
TS
MTS (no s^{4}U)
HPDP (no s^{4}U)
TS (no s^{4}U)
Input (50%)
one s^{4}U
no s^{4}U
μM biotin-SR
39 nt

Figure S2

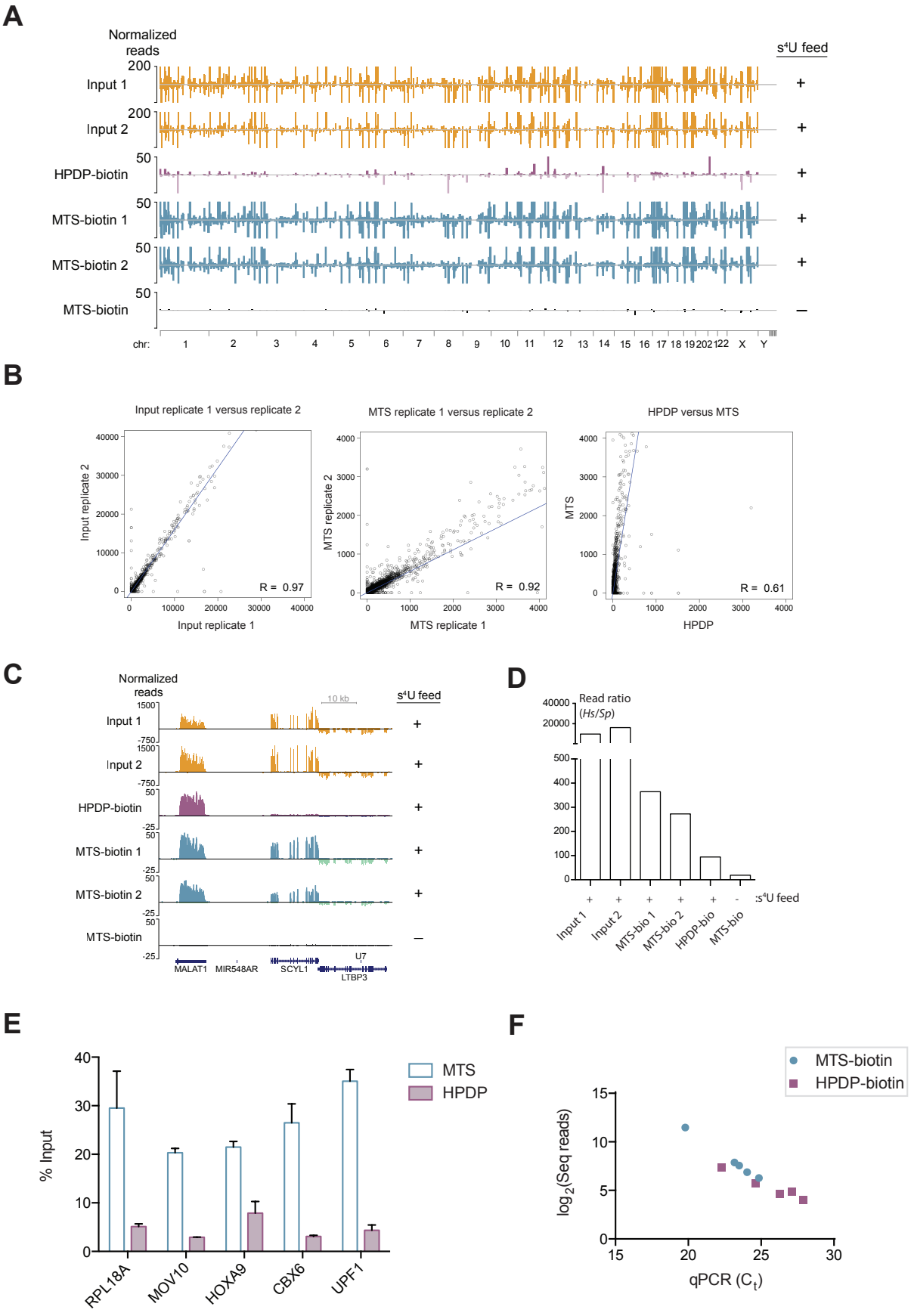
A
Normalized reads
s4U feed
Input 1
Input 2
HPDP-biotin
MTS-biotin 1
MTS-biotin 2
MTS-biotin
chr:
B
Input replicate 1 versus replicate 2
R = 0.97
Input replicate 1
Input replicate 2
MTS replicate 1 versus replicate 2
R = 0.92
MTS replicate 1
MTS replicate 2
HPDP versus MTS
R = 0.61
HPDP
MTS
C
Normalized reads
10 kb
s4U feed
MALAT1
MIR548AR
SCYL1
U7
LTBP3
D
Read ratio (Hs/Sp)
s4U feed
Input 1
Input 2
MTS-bio 1
MTS-bio 2
HPDP-bio
MTS-bio
E
% Input
MTS
HPDP
RPL18A
MOV10
HOXA9
CBX6
UPF1
F
MTS-biotin
HPDP-biotin
log2(Seq reads)
qPCR (Ct)

Figure S3

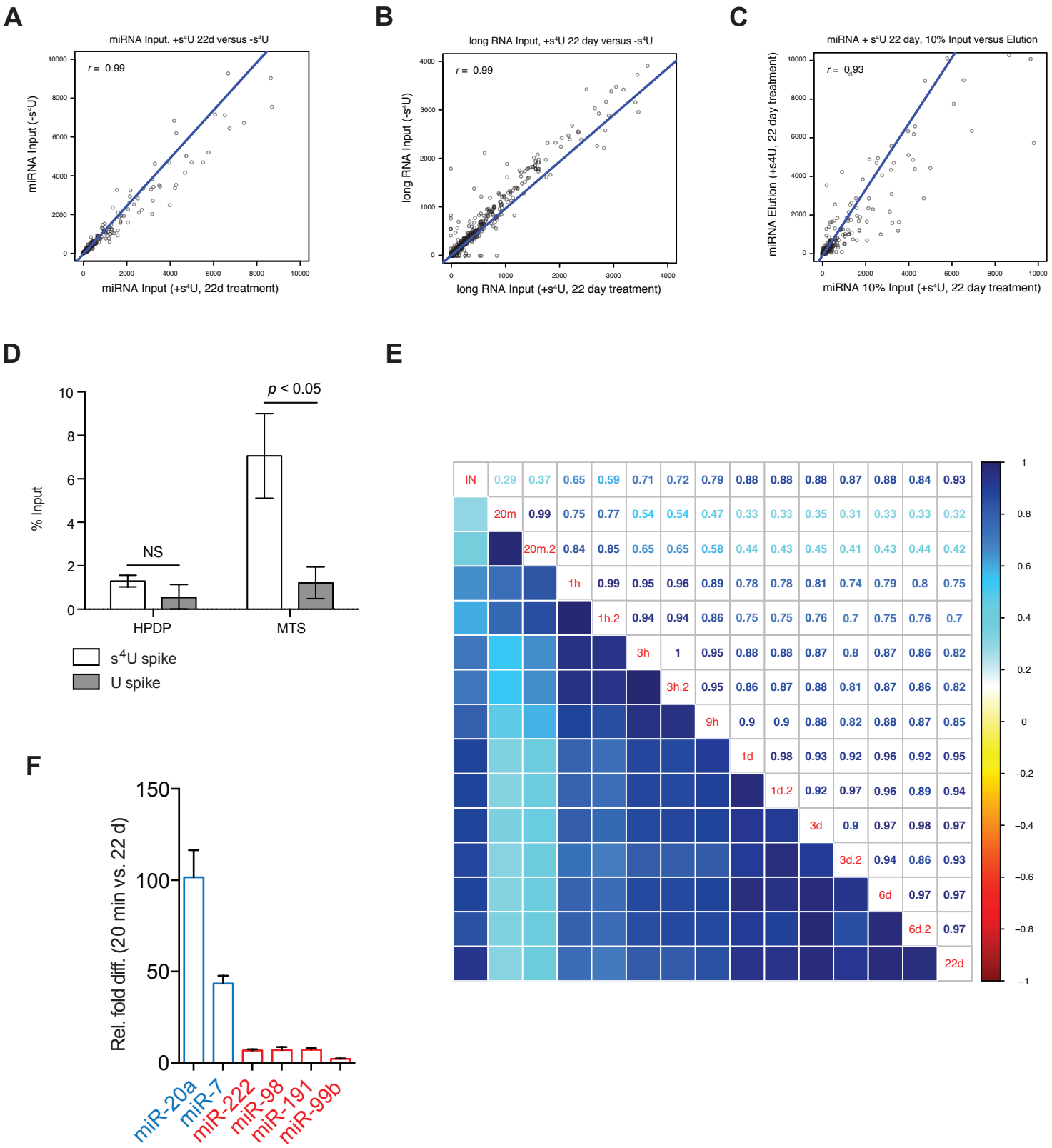
A
miRNA Input, +s4U 22d versus -s4U
r = 0.99
miRNA Input (-s4U)
miRNA Input (+s4U, 22d treatment)
B
long RNA Input, +s4U 22 day versus -s4U
r = 0.99
long RNA Input (-s4U)
long RNA Input (+s4U, 22 day treatment)
C
miRNA + s4U 22 day, 10% Input versus Elution
r = 0.93
miRNA Elution (+s4U, 22 day treatment)
miRNA 10% Input (+s4U, 22 day treatment)
D
p < 0.05
NS
% Input
HPDP
MTS
s4U spike
U spike
E
IN 0.29 0.37 0.65 0.59 0.71 0.72 0.79 0.88 0.88 0.88 0.87 0.88 0.84 0.93
20m 0.99 0.75 0.77 0.54 0.54 0.47 0.33 0.33 0.35 0.31 0.33 0.33 0.32
20m.2 0.84 0.85 0.65 0.65 0.58 0.44 0.43 0.45 0.41 0.43 0.44 0.42
1h 0.99 0.95 0.96 0.89 0.78 0.78 0.81 0.74 0.79 0.8 0.75
1h.2 0.94 0.94 0.86 0.75 0.75 0.76 0.7 0.75 0.76 0.7
3h 1 0.95 0.88 0.88 0.87 0.8 0.87 0.86 0.82
3h.2 0.95 0.86 0.87 0.88 0.81 0.87 0.86 0.82
9h 0.9 0.9 0.88 0.82 0.88 0.87 0.85
1d 0.98 0.93 0.92 0.96 0.92 0.95
1d.2 0.92 0.97 0.96 0.89 0.94
3d 0.9 0.97 0.98 0.97
3d.2 0.94 0.86 0.93
6d 0.97 0.97
6d.2 0.97
22d
F
Rel. fold diff. (20 min vs. 22 d)
miR-20a
miR-7
miR-222
miR-98
miR-191
miR-99b

SUPPLEMENTAL FIGURE AND TABLE LEGENDS

Figure S1. Reactivity of activated disulfides with s^4U and *in vitro* modulation of bias in MTS- and HPDP-biotin enrichments, related to Figure 1

(A) ^1H NMR spectrum of s^4U alone. Peak labeled with a red "*" corresponds to the starred proton in the s^4U structure. (B) ^1H NMR spectrum of s^4U when treated with methane methylthiolsufonate (MeMTS), the same reactive disulfide of MTS-biotin. MeMTS was incubated with s^4U for 30 min and the extent of disulfide exchange was monitored by the chemical shift in proton labeled with a red "*". Peak labeled with a blue "*" represents the chemical shift upon disulfide bond formation. (C) ^1H NMR spectrum of s^4U when treated with a compound containing the same functional group of HPDP-biotin. 3-[2-Pyridyldithio]propionyl hydrazide (PDPH) was incubated with s^4U for 2 hr and the extent of disulfide exchange was monitored by changes in chemical shift as in (B). (D) RNA from *E. coli* K-12 cells was reacted with MTS-TAMRA fluorescent dye and visualized on a 5% urea-PAGE gel. K-12 cells express ThiI, an enzyme that selectively modifies U8 of tRNA to s^4U8 (Mueller et al., 1998b). RNA from a Δ*thiI* knockout shows little TAMRA signal (traces of unmethylated 2-thiouridine on tRNA can still react), whereas a strong TAMRA signal is present in the K-12 cells only in tRNA. Total RNA was stained with GelGreen. (E) Schematic of *in vitro* enrichment of s^4U-RNA using an RNA ladder. An RNA ladder was *in vitro* transcribed with Cy5-CTP and with or without added s^4UTP. s^4U-RNAs were enriched by reacting with disulfide-activated biotin derivatives using either HPDP, MTS, or thiolsulfonate (TS, an alternative disulfide activated biotin reagent) chemistry. (F) Input, flow-through, and elution RNAs were analyzed by urea-PAGE and visualized by Cy5 fluorescence. Band intensities were quantified using ImageJ. (G) Comparison

between the yields observed in (E) and expected enrichment using models that assume different biotinylation efficiencies. In all cases modeled lines assume ratio of s^4U/U_{total} = 0.075 to determine the expected yield given different biotinylation efficiencies (y_{bio}) based on the equation:

$$\text{yield RNA} = \sum_{j=0}^{N_i} \left[1 - (1 - y_{bio})^j\right] p(U_i = j)$$

(see also the "Modeling expected yields" section of the Detailed Protocol). In comparison to the models results, empirical yields using the band intensities from (B) were plotted based on transcript length. (H) Effects of biotin concentration on modeled s^4U-RNA enrichment. Synthetic short RNAs (1 nM) with one s^4U residue (red) or zero s^4U residues (green) were enriched by 200 μM (comparable to 50 μg biotin in total RNA pulldown) or 20 μM HPDP- or MTS-biotin. No significant difference in enrichment was observed using these two concentrations of MTS-biotin eluent, whereas 200 μM HPDP-biotin showed 6-fold greater enrichment over 20 μM HPDP-biotin.

Figure S2. Reproducibility of MTS-biotin enrichment, related to Figure 2

(A) Whole genome alignments of RNA-Seq samples as in Figure 2B. The *y*-axis indicates the number of reads normalized to total number of *S. pombe* aligned reads. To compare coverage between samples using the same scale on the *y*-axis, in many cases read coverage exceeds the *y*-axis upper limit in Input (135 cases), MTS-biotin (127 cases) and HPDP-biotin (4 cases). Chromosomes are indicated below the mapped reads. (B) Scatter plots and Pearson correlations of normalized FPKM values for *H. sapiens* transcript isoforms. Plots show Input 1 vs. Input 2 (left), MTS-biotin replicate 1 vs. HPDP-biotin (center), and MTS-biotin replicate 1 vs. MTS-biotin replicate 2 (right). (C) Example of genes enriched by HPDP-biotin and MTS-biotin as in

Figure 2C. (D) Total reads for each RNA-Seq sample that mapped to the *H. sapiens* genome, normalized by total number of reads that mapped to the *S. pombe* genome, as in Figure 2D. (E) Samples enriched by MTS- or HPDP-biotin from RNA-seq submission were analyzed by qPCR using gene-specific primers for RPL18A, MOV10, HOXA9, CBX6, and UPF1 with two replicates. C_t values from qPCR were used to calculate percent input using the equation:

$$\frac{1}{2^{(Ct_{sample}-Ct_{input})}}$$

where the input is the average of two replicates. Error bars indicate the mean of two technical replicates +/- SEM. (F) C_t values from qPCR were plotted against the number of reads (log_2 transformed) for deep sequencing in input (triangles), MTS- (circles) and HPDP- (squares) enriched samples.

Figure S3. Analysis of s^4U metabolic labeling and enrichment for miRNA RATE-Seq, related to Figure 3

(A-C) Scatter plots and Pearson correlations of RNA-Seq quantifications of *H. sapiens* miRNA transcripts. Plots show (A) reads from miRNA isolated from cells with not s^4U treatment compared to reads from total miRNA from cells after 22 days of s^4U treatment; (B) analysis of long RNAs from the same cells as in (A); and (C) analysis of miRNA isolated from 22 day s^4U treatment (10% input) vs. MTS-biotin enriched miRNA from 22 days of s^4U treatment. (D) miRNAs enriched with HPDP- and MTS-biotin. Control miRNA spikes containing one s^4U (EED004r) or zero s^4U (EED0095r) were enriched with s^4U-miRNA samples and enrichment was detected by qPCR using the same equation as above. The s^4U-containing spike-in control was not significantly enriched over background by HPDP-biotin (p = 0.27), whereas the s^4U-containing spike-in control was significantly enriched by MTS-biotin (p = 0.034). (E) Heatmap

similar to Figure 3C with annotated correlation coefficients (Pearson's *r*) between miRNA levels at different times after s^4U treatment. Replicate samples are indicated by (rep). (F) The enrichment of select miRNAs using MTS-biotin after 1 hr and 6 days s^4U treatment was validated by qPCR and quantified as fold enrichment as in Figure S2E. Error bars indicate the mean of three technical replicates +/- SEM.

Table S1. RNA-Seq alignment statistics

Table S2. Fast-turnover miRNAs that have previously been reported to be stable when transcription is inhibited. A list of miRNAs determined to be fast turnover (see Figure 3E), and their turnover rates (% turnover) in experiments where miRNA levels are monitored following transcriptional blockade (Bail et al., 2010; Guo et al., 2015).

Table S3. Oligonucleotide sequences. Names indicate internal spike codes (in the case of RNA synthetic spike), or target primer sequences (in the case of DNA qPCR primers). RNA synthetic spikes are synthetic RNA sequences containing either zero or one s^4U nucleotides that were included during s^4U-miRNA enrichment and sequencing (see Experimental Procedures). DNA qPCR primers were designed from sequences provided in Gregersen *et al.* 2014.

SUPPLEMENTAL REFERENCES

Borowski, L., and Szczesny, R. (2014). Measurement of mitochondrial RNA stability by metabolic labeling of transcripts with 4-thiouridine. Method. Mol. Biol. *1125*, 277-286.

Burger, K., Mühl, B., Kellner, M., Rohrmoser, M., Gruber-Eber, A., Windhager, L., Friedel, C., Dölken, L., and Eick, D. (2013). 4-thiouridine inhibits rRNA synthesis and causes a nucleolar stress response. RNA Biol. *10*, 1623-1630.

Cleary, M. (2008). Cell type-specific analysis of mRNA synthesis and decay in vivo with uracil phosphoribosyltransferase and 4-thiouracil. Method. Enzymol. *448*, 379-406.

Cosker, K., Pazyra-Murphy, M., Fenstermacher, S., and Segal, R. (2013). Target-derived neurotrophins coordinate transcription and transport of bclw to prevent axonal degeneration. J. Neurosci. *33*, 5195-5207.

Dölken, L., Ruzsics, Z., Rädle, B., Friedel, C., Zimmer, R., Mages, J., Hoffmann, R., Dickinson, P., Forster, T., Ghazal, P.*, et al.* (2008). High-resolution gene expression profiling for simultaneous kinetic parameter analysis of RNA synthesis and decay. RNA *14*, 1959-1972.

Eser, P., Demel, C., Maier, K., Schwalb, B., Pirkl, N., Martin, D., Cramer, P., and Tresch, A. (2014). Periodic mRNA synthesis and degradation co-operate during cell cycle gene expression. Mol. Syst. Biol. *10*, 717.

Friedel, C., and Dölken, L. (2009). Metabolic tagging and purification of nascent RNA: implications for transcriptomics. Mol. Biosyst. *5*, 1271-1278.

Friedel, C., Dölken, L., Ruzsics, Z., Koszinowski, U., and Zimmer, R. (2009). Conserved principles of mammalian transcriptional regulation revealed by RNA half-life. Nucleic Acids Res. *37*, e115.

Gay, L., Miller, M., Ventura, P., Devasthali, V., Vue, Z., Thompson, H., Temple, S., Zong, H., Cleary, M., Stankunas, K.*, et al.* (2013). Mouse TU tagging: a chemical/genetic intersectional method for purifying cell type-specific nascent RNA. Genes Dev. *27*, 98-115.

Harrow, J., Frankish, A., Gonzalez, J., Tapanari, E., Diekhans, M., Kokocinski, F., Aken, B., Barrell, D., Zadissa, A., Searle, S.*, et al.* (2012). GENCODE: the reference human genome annotation for The ENCODE Project. Genome Res. *22*, 1760-1774.

Heyn, P., Kircher, M., Dahl, A., Kelso, J., Tomancak, P., Kalinka, A., and Neugebauer, K. (2014). The earliest transcribed zygotic genes are short, newly evolved, and different across species. Cell Rep. *6*, 285-292.

Iadevaia, V., Zhang, Z., Jan, E., and Proud, C. (2012). mTOR signaling regulates the processing of pre-rRNA in human cells. Nucleic Acids Res. *40*, 2527-2539.

Miller, C., Schwalb, B., Maier, K., Schulz, D., Dümcke, S., Zacher, B., Mayer, A., Sydow, J., Marcinowski, L., Dölken, L.*, et al.* (2011). Dynamic transcriptome analysis measures rates of mRNA synthesis and decay in yeast. Mol. Syst. Biol. 10.1038/msb.2010.112.

Mueller, E., Buck, C., Palenchar, P., Barnhart, L., and Paulson, J. (1998a). Identification of a gene involved in the generation of 4-thiouridine in tRNA. Nucleic Acids Res. *26*, 2606-2610.

Mueller, E.G., Buck, C.J., Palenchar, P.M., Barnhart, L.E., and Paulson, J.L. (1998b). Identification of a gene involved in the generation of 4-thiouridine in tRNA. Nucleic Acids Res. *26*, 2606-2610.

Neymotin, B., Athanasiadou, R., and Gresham, D. (2014). Determination of in vivo RNA kinetics using RATE-seq. RNA *20*, 1645-1652.

Pena, A., Pimentel, M., Manso, H., Vaz-Drago, R., Pinto-Neves, D., Aresta-Branco, F., Rijo-Ferreira, F., Guegan, F., Pedro Coelho, L., Carmo-Fonseca, M.*, et al.* (2014). Trypanosoma

brucei histone H1 inhibits RNA polymerase I transcription and is important for parasite fitness in vivo. Mol. Microbiol. *93*, 645-663.

Popova, A., and Williamson, J. (2014). Quantitative analysis of rRNA modifications using stable isotope labeling and mass spectrometry. J. Am. Chem. Soc. *136*, 2058-2069.

Rabani, M., Raychowdhury, R., Jovanovic, M., Rooney, M., Stumpo, D.J., Pauli, A., Hacohen, N., Schier, A.F., Blackshear, P.J., Friedman, N.*, et al.* (2014). High-resolution sequencing and modeling identifies distinct dynamic RNA regulatory strategies. Cell *159*, 1698-1710.

Rüegger, S., and Großhans, H. (2012). MicroRNA turover: when, how, and why. Trends Biochem. Sci. *37*, 436-446.

Schulz, D., Pirkl, N., Lehmann, E., and Cramer, P. (2014). Rpb4 subunit functions mainly in mRNA synthesis by RNA polymerase II. The Journal of biological chemistry *289*, 17446-17452.

Schwanhäusser, B., Busse, D., Li, N., Dittmar, G., Schuchhardt, J., Wolf, J., Chen, W., and Selbach, M. (2011). Global quantification of mammalian gene expression control. Nature *473*, 337-342.

Sun, M., Schwalb, B., Pirkl, N., Maier, K., Schenk, A., Failmezger, H., Tresch, A., and Cramer, P. (2013). Global analysis of eukaryotic mRNA degradation reveals Xrn1-dependent buffering of transcript levels. Mol. Cell *52*, 52-62.

Sun, M., Schwalb, B., Schulz, D., Pirkl, N., Etzold, S., Larivière, L., Maier, K., Seizl, M., Tresch, A., and Cramer, P. (2012). Comparative dynamic transcriptome analysis (cDTA) reveals mutual feedback between mRNA synthesis and degradation. Genome Res. *22*, 1350-1359.

Zeiner, G., Cleary, M., Fouts, A., Meiring, C., Mocarski, E., and Boothroyd, J. (2008). RNA analysis by biosynthetic tagging using 4-thiouracil and uracil phosphoribosyltransferase. Method. Mol. Biol. *419*, 135-146.